中国科学院国家空间科学中心
National Space Science Center . CAS

Koninklijk Nederlands
Meteorologisch Instituut
Ministerie van Infrastructuur en Waterstaat

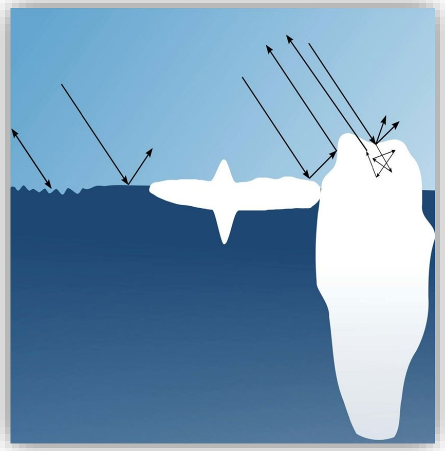

The Quality Control Indicator *Joss* on Ku-band Wind Scatterometry for Sea Ice Applications with Reference to C-band, Passive Measurements and Precipitations

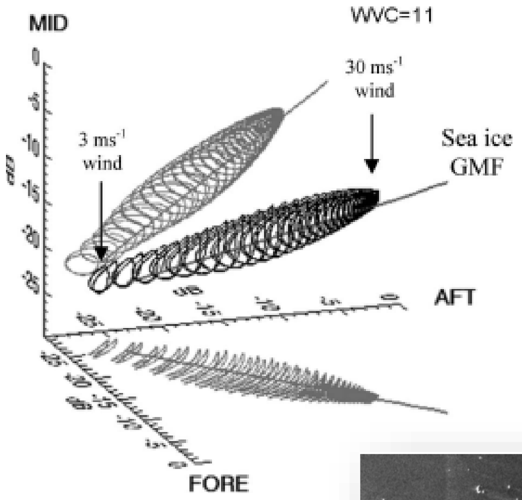

Xingou Xu [1], Ad Stoffelen [2]✉

1 National Space Science Center, Chinese Academy of Sciences
2 Royal Netherlands Meteorological Institute (KNMI)
✉ ad.stoffelen@knmi.nl

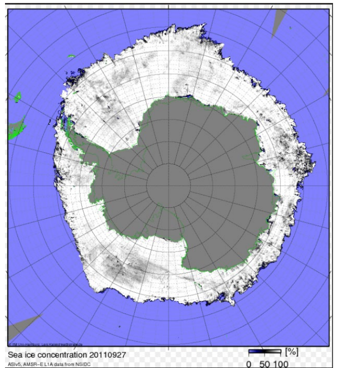

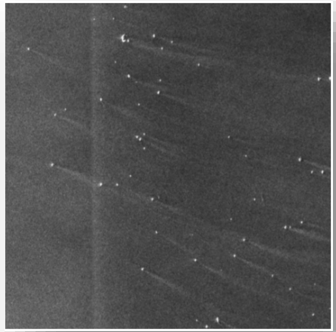

IOVWST 2023. Nanjing, Jiangsu, China. 1st, Dec.

The Scatterometer Ice GMFs

The ice GMFs

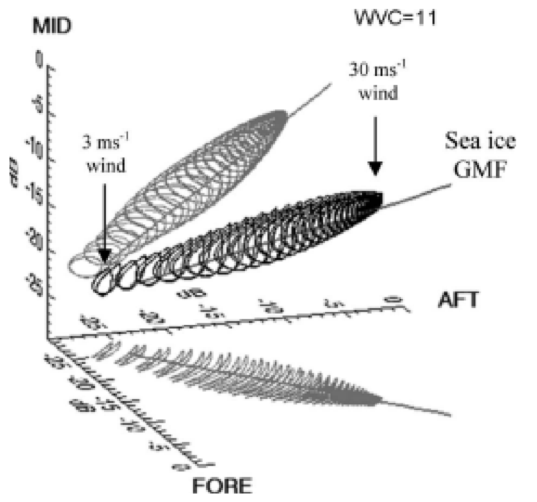

Geophysical model functions (GMFs) for ocean wind and sea ice backscatter at C-band V-pol in the 3-D space of ASCAT measurements for a mid-swath WVC. The ocean wind GMF is a tube-shaped manifold depicted here as a function of wind speed (3–30 ms^{-1} in steps of 1 ms^{-1}) and direction. The sea ice GMF is a straight line with azimuthal (AFT/FORE) symmetry, depicted as a function of sea ice normalized backscatter.

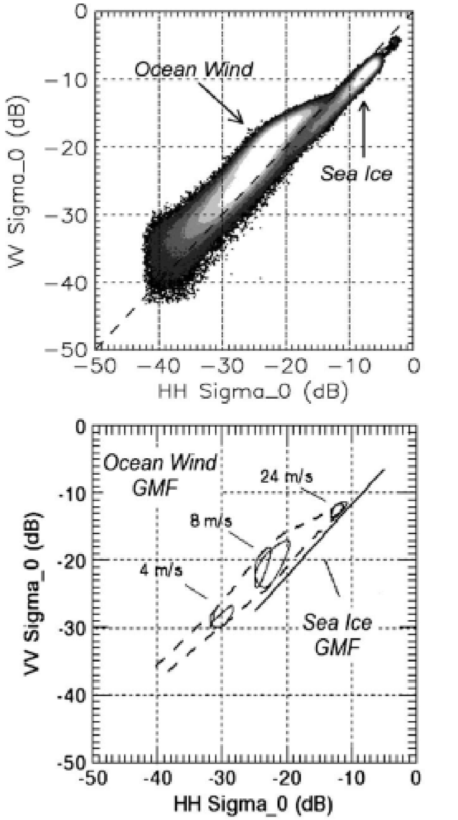

$\{\sigma^0_{wind}\} = \mathbf{GMF_{wind}}$ (wind speed, wind direction, WVC)

$\{\sigma^0_{ice}\} = \mathbf{GMF_{ice}}$ (ice brightness)

(Top) Observed distribution of backscatter and (bottom) empirical ocean wind and sea ice model functions in the space of QuikSCAT measurements (projection on the for/aft planes).

- The Ice GMFs are obtained from pure ice surfaces, with references to wind GMF in speed.

- Sea ice backscatter shows no directional preference in azimuth, tightly conforming to a 1-D straight-line model that features sea ice brightness (or proxy sea ice age) as its only independent variable

- The function does not change with time or geographical location

(Belmonte et al., 2012; R. Belmonte, A .Stoffelen et. al, 2011)

Identification of sea ice in the ocean from wind scatterometers

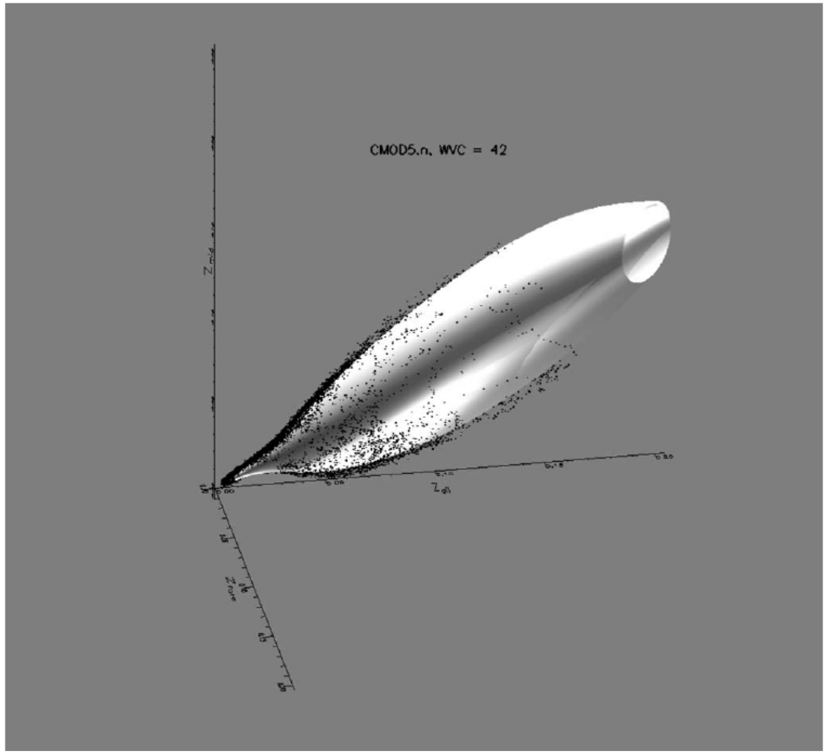

Visualization of CMOD5.n and the ASCAT triplets (dots) in 3-D measurement space for WVC number 42 for wind speeds up to 30 m / s (Jeroen Verspeek, Ad Stoffelen, Marcos Portabella, Hans Bonekamp, Craig Anderson, and Julia Figa Saldaña. 2009)

MLE: Weighted Euclidian distance to the wind cone or sea ice line

$$MLE = \frac{1}{N}\sum_{i}^{N}\frac{\left(\sigma_i^o - \sigma_{sim_i}\right)^2}{\left(K_{pi} \bullet \sigma_i\right)^2}$$

σ_i^o is the ith NRCS of the N NRCSs within a Wind Vector Cell (WVC),
K_{pi} represents the variance of σ_i^o in it.
σ_{sim_i} is from a wind or sea ice GMF using observing geometry and local wind vector or sea ice information.

MLE quantifies NRCS deviations from wind GMF, *and are used for Bayesian inference of sea ice together with ice GMF*

(Marcos Portabella and Ad Stoffelen, 2006; Belmonte and Stoffelen, 2011)

The indicator J_{oss}

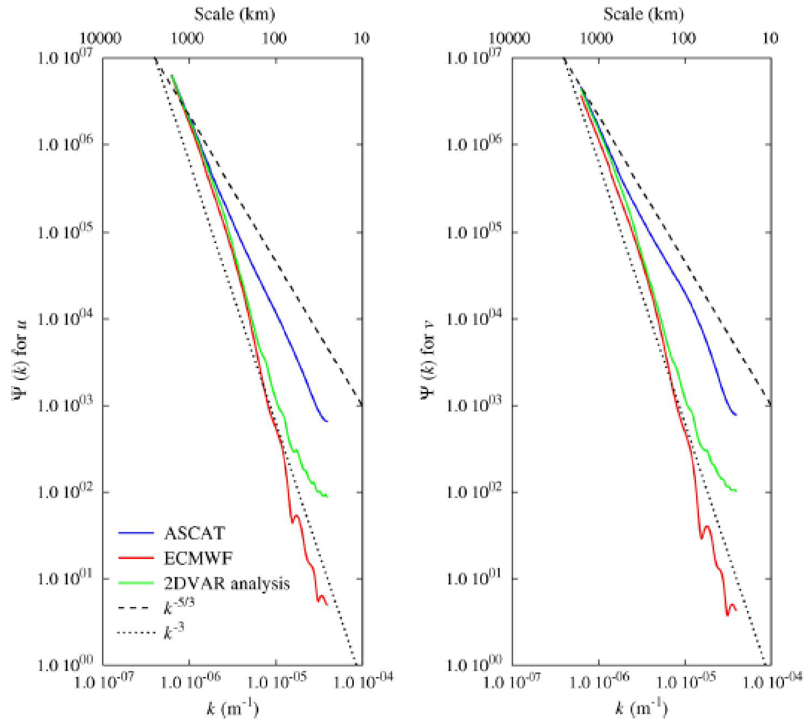

Wind component spectra obtained from all ASCAT-12.5 data of January 2009. A variational data assimilation scheme based on statistical interpolation acts as a low-pass filter.(Jur Vogelzang, Ad Stoffelen. 2011)

2DVAR is used for ambiguity removal on the basis of a spatial wind field analysis J_{oss}, the local difference in speed of the selected wind ambiguity and the analysis wind speed, naturally locates and quantifies local disturbances.

$$J_{oss} = f - f_S$$

f_S. is the 2DVAR analysis wind speed at a WVC,
f. is the local WVC-selected wind speed.

(Xingou Xu, Ad Stoffelen 2020)

J_{oss} measures heterogeneity of the WVC

Method:

- The differences of NRCS with wind GMF represented by MLE in different frequencies
- The heterogeneity of the averaged scene represented by J_{oss}.
- Different features of MLE and J_{oss} for ice screening and smaller scale iceberg detection with references from different sources

Data descriptions

Scatterometer data: Collocation of Ku-band and C-band Scatterometer from OSCAT-2, ASCAT-A and ASCAT-B (from 2016-2019)

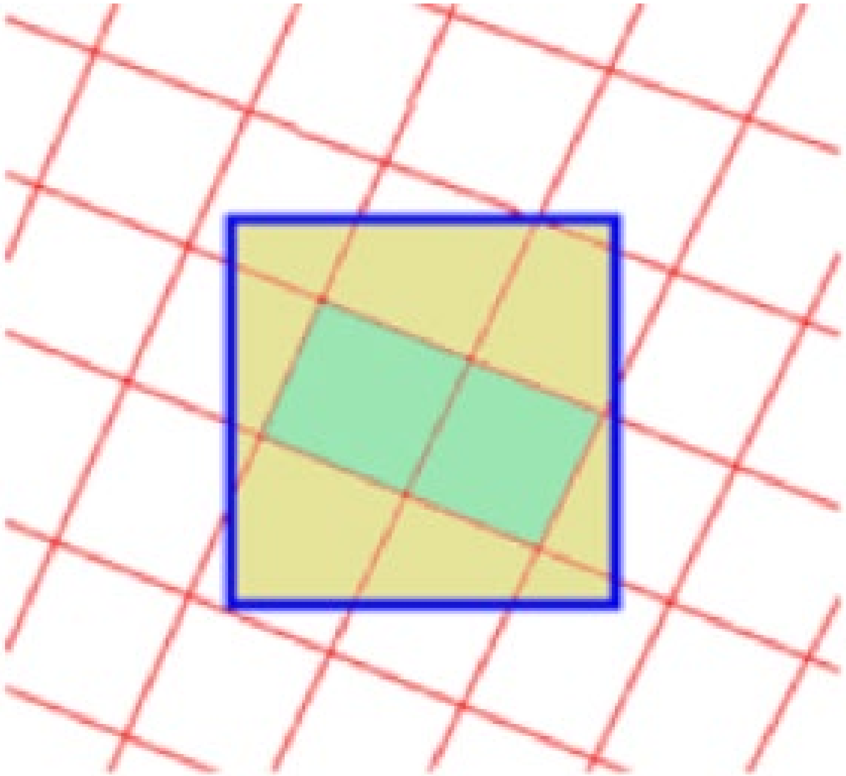

Illustration of area-weight collocating for SIC and rain rates, a circle is used instead of the blue WVC (X. Xu et al., 2020)

Other information applied:

- Sea Ice Concentration: AMSR-E
- Iceberg information: the Sentinel-1.
- Surface Rain Rates: GPM final run

MLE, J_{oss}, and SIC from collocated Ku and C-band observations

- C band *MLE* has been well applied for sea ice identification
- Verification of ice screening for Ku band J_{oss} and compared with C band *MLE*

QC- all:

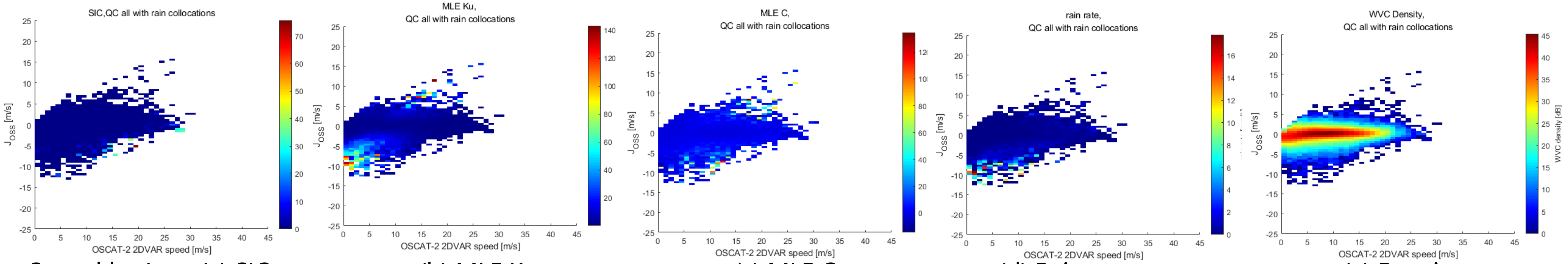

Sorted by Joss: (a) SIC (b) MLE Ku (c) MLE C (d) Rain rate (e) Density

QC- II (Ku- rejection, C acceptance):

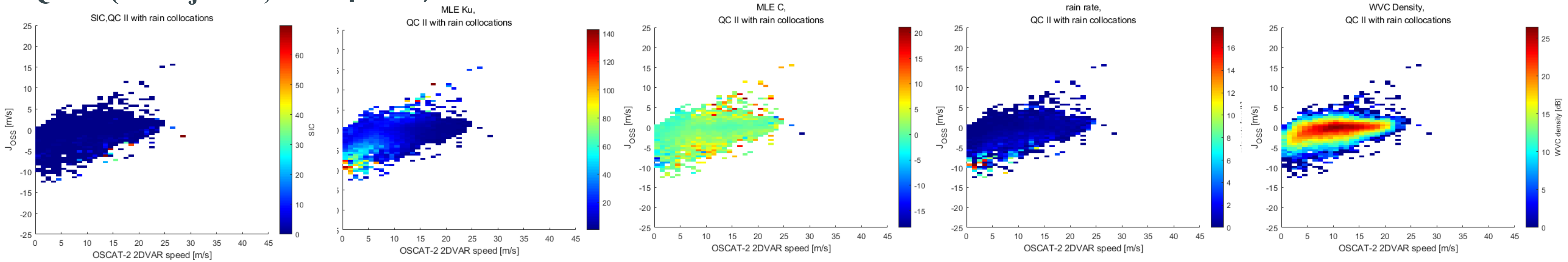

Sorted by Joss: (a) SIC (b) MLE Ku (c) MLE C (d) Rain rate (e) Density

MLE, J_{oss}, and SIC from Ku band observations

- HY-2B Ku band J_{oss}

QC- all:

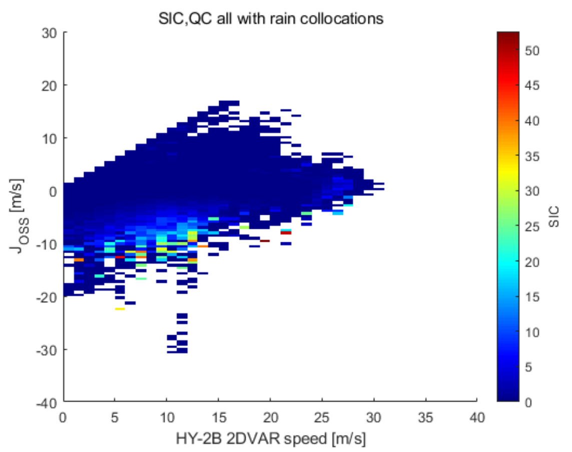

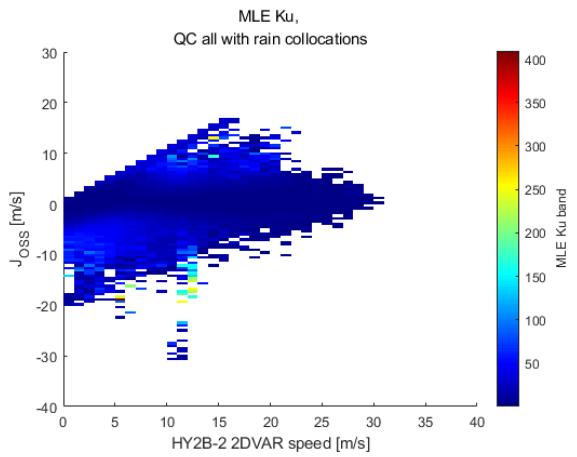

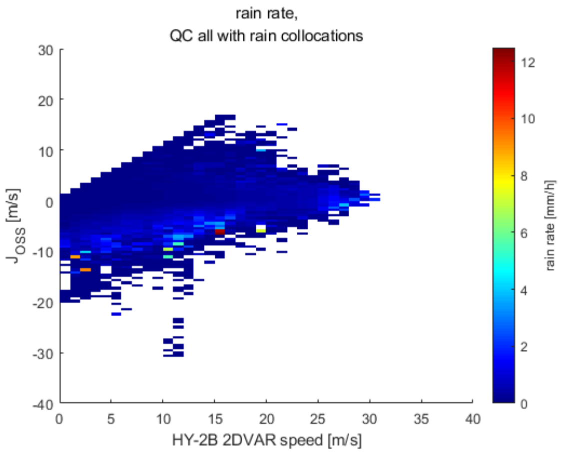

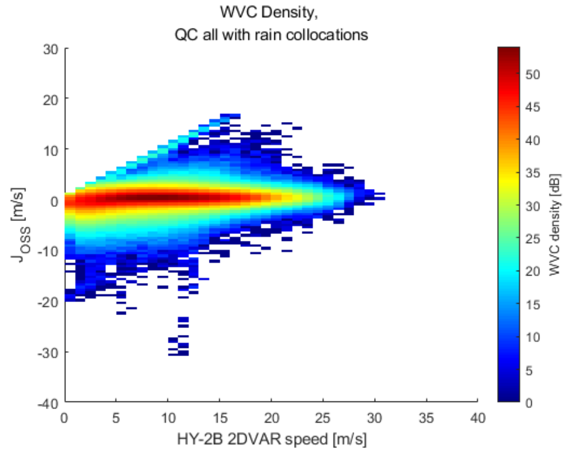

Sorted by Joss: (a) SIC (b) MLE Ku (c) Rain rate (d) Density

QC- rejection:

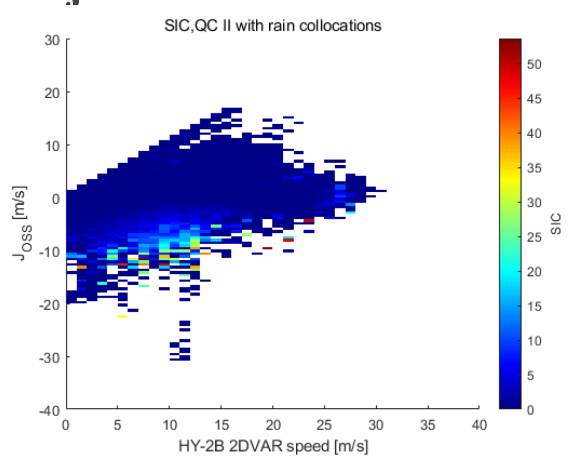

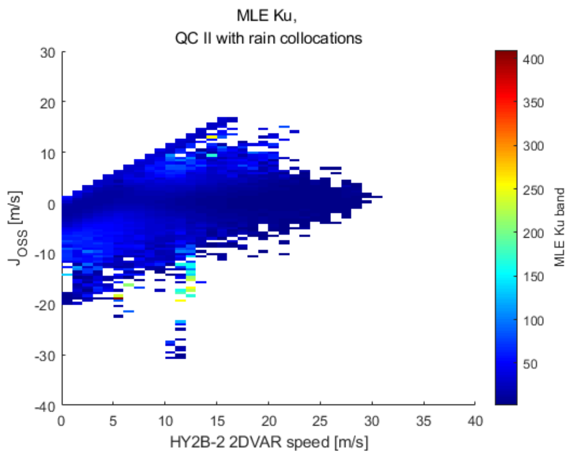

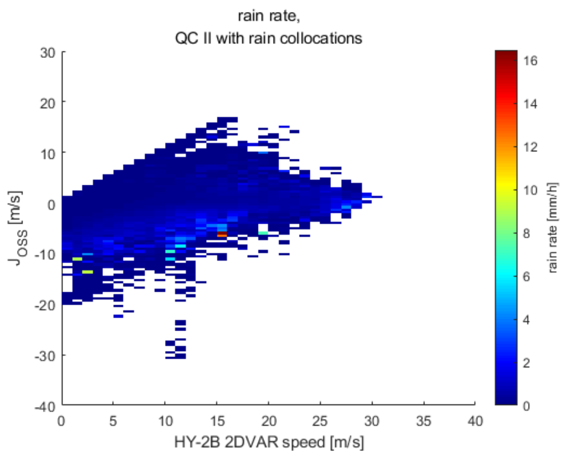

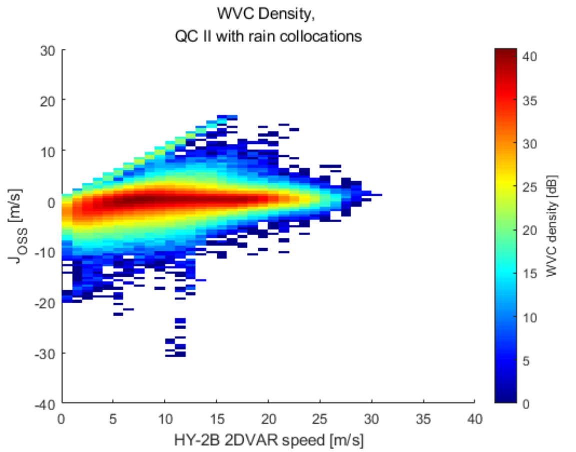

Sorted by Joss: (a) SIC (b) MLE Ku (c) Rain rate (d) Density

Summary for MLE, J_{oss}, and SIC from collocated Ku and C-band observations

- Low to medium wind speed, effects of SIC similar with rains, in higher wind speeds SIC affect more often for high latitude
- MLE good in identifying rains and SIC, both C band and Ku band MLE more sensitive to SIC than rains, while C MLE is more likely to be linked with sea ice.
- The indicator J_{oss} compantary to *MLE* flags

Ku band scatterometer MLE and Joss v.s. SAR iceberg

- *A* case

-The potential large sic set is obtained *under the condition* (white line):

$$J_{oss} \leqslant 0.33 f - 5$$

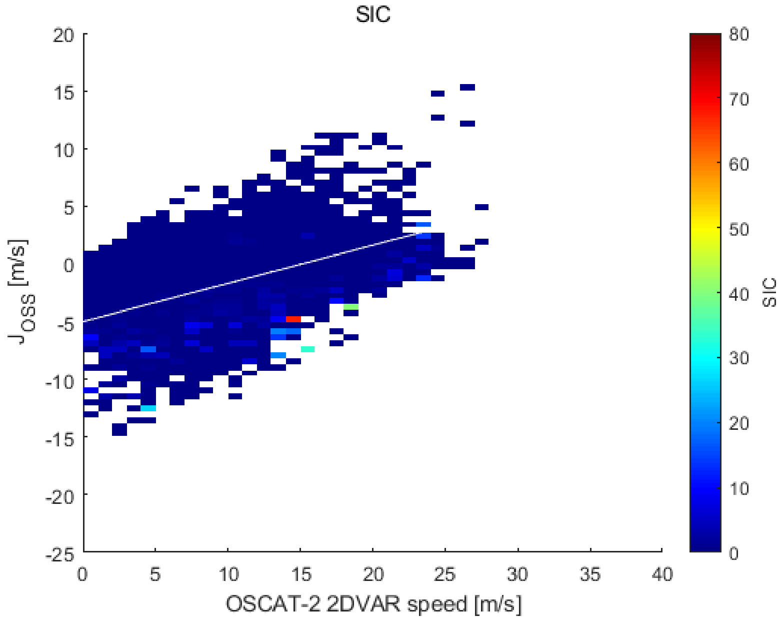

-A specific iceberg case between Greenland and Canada:

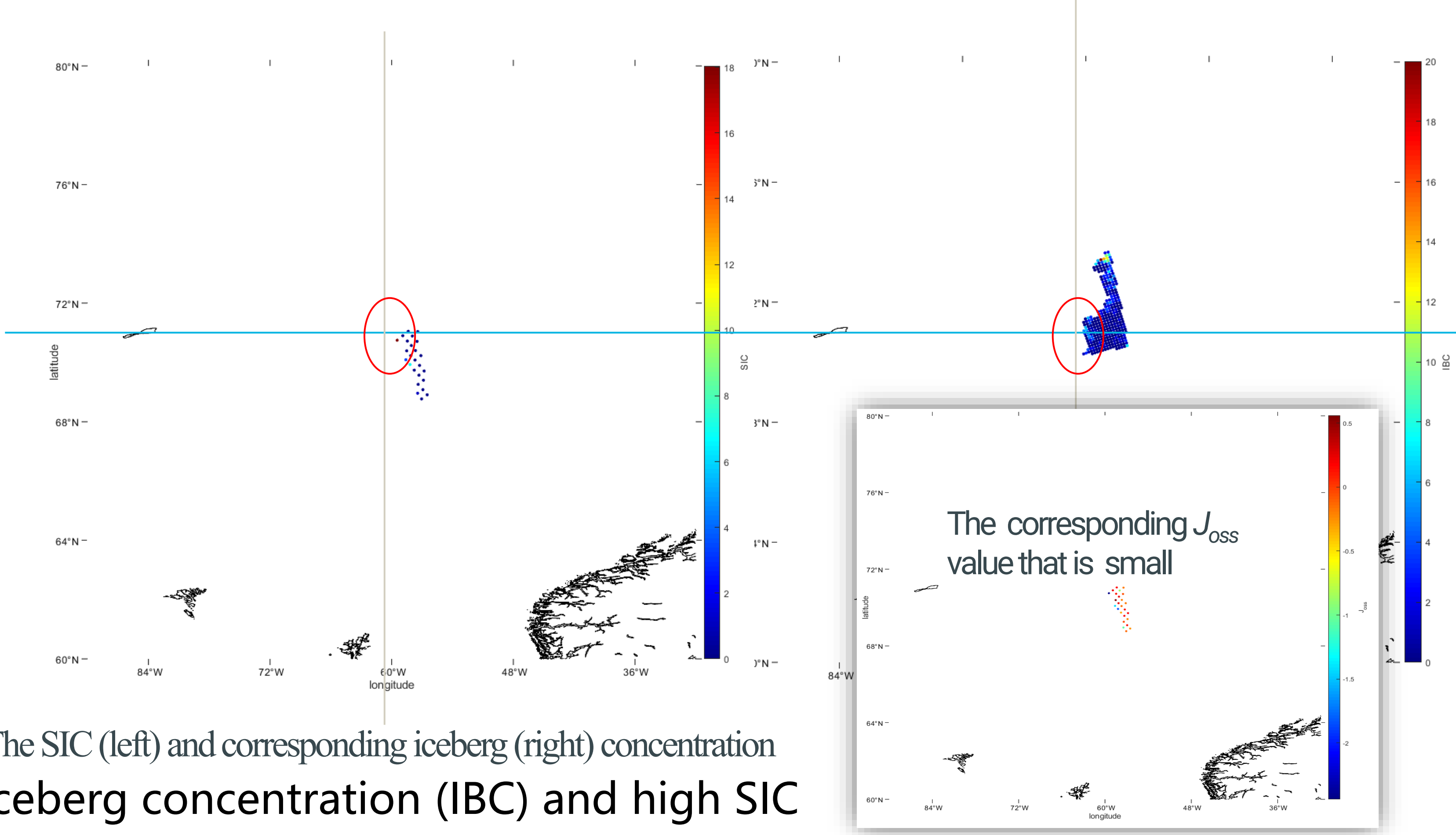

The SIC (left) and corresponding iceberg (right) concentration

Low Joss values corresponds to high iceberg concentration (IBC) and high SIC

Ku band scatterometer MLE and Joss v.s. SAR iceberg

- *Statistics*

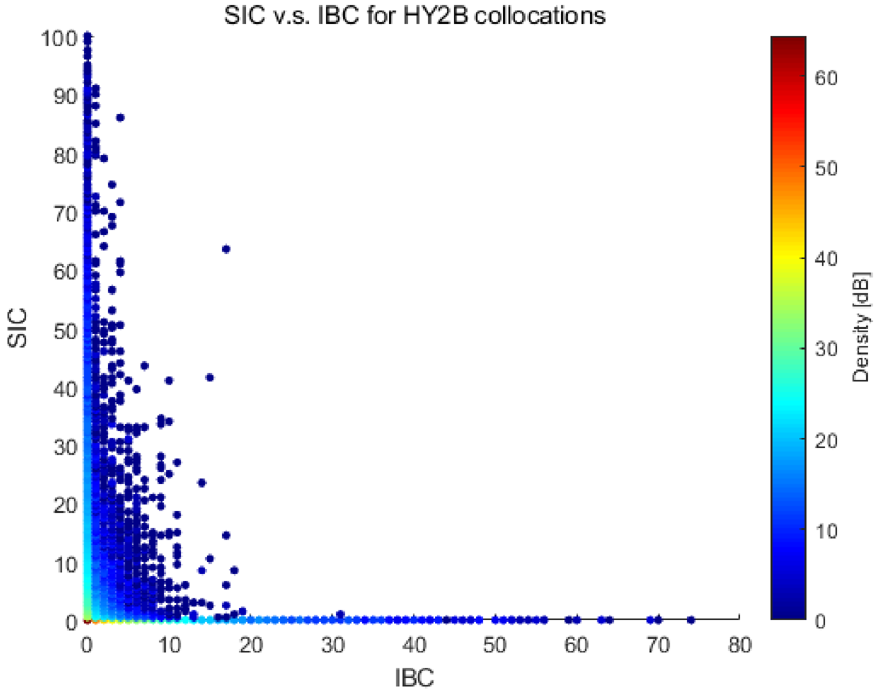

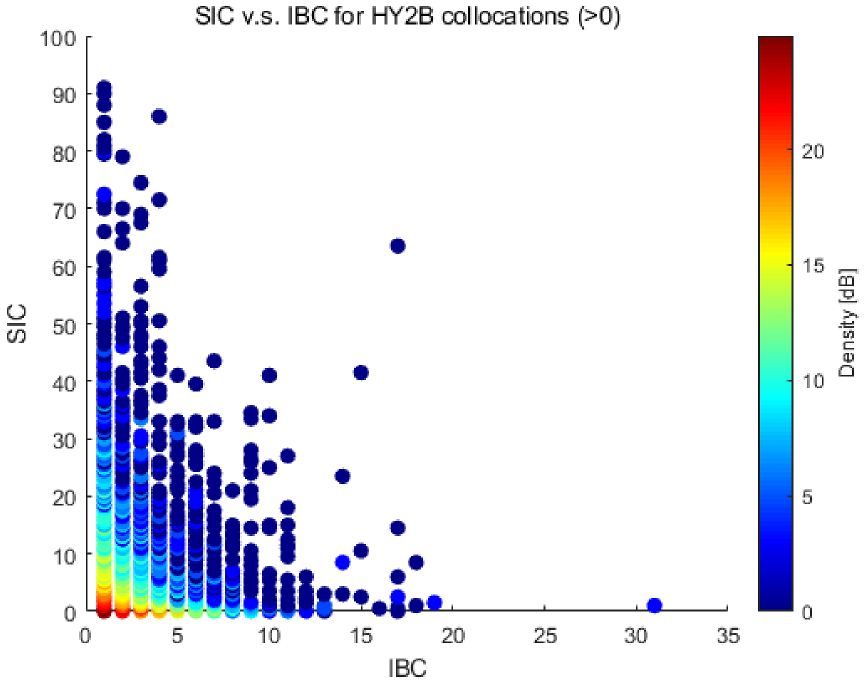

SIC and IBC are different in different observations and not in good correlation

Ku band scatterometer MLE and Joss v.s. SAR iceberg

- *Statistics*

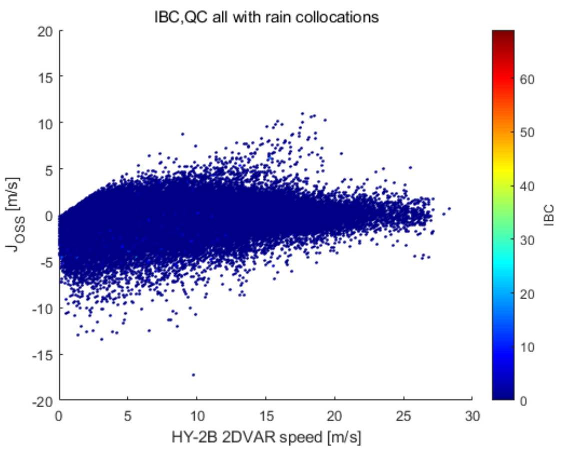

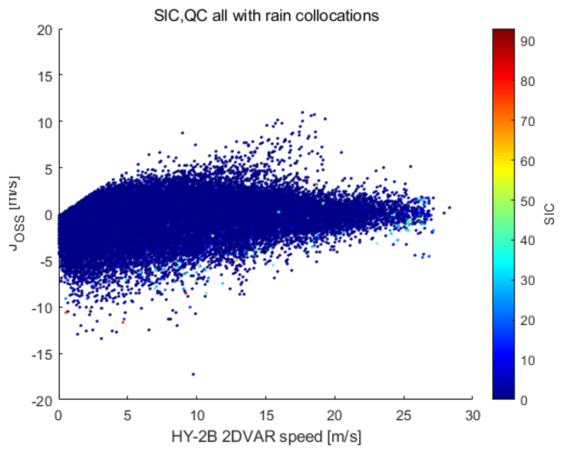

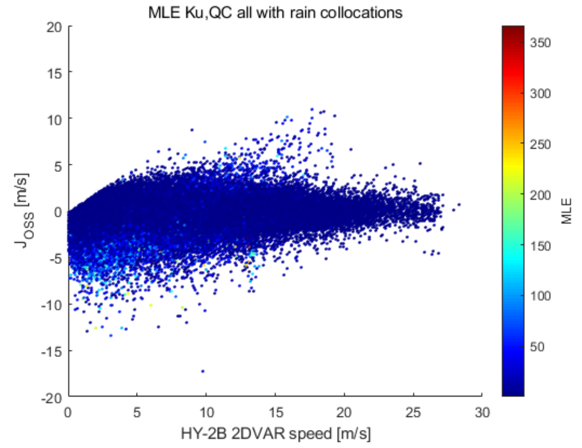

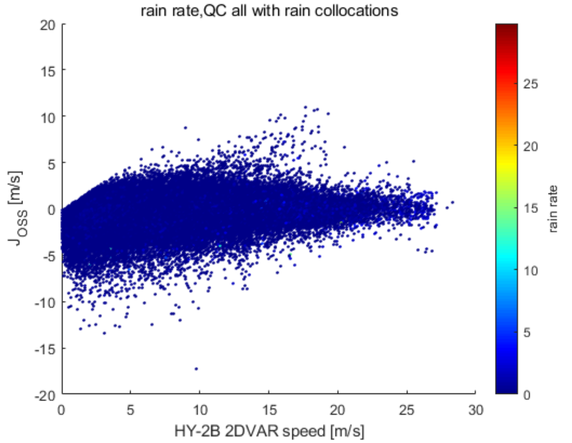

Sorted by Joss: (a) IBC (b) SIC (c) MLE (d) Rain rate

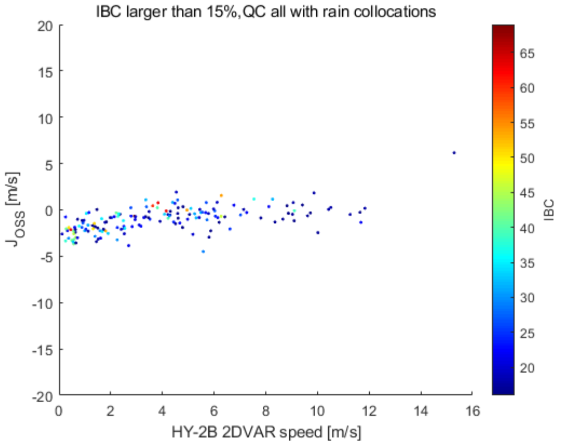

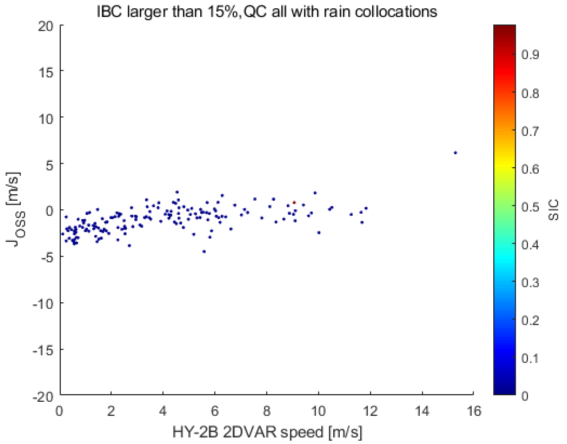

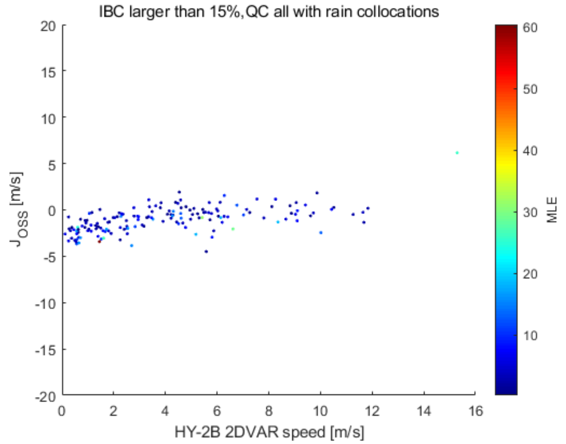

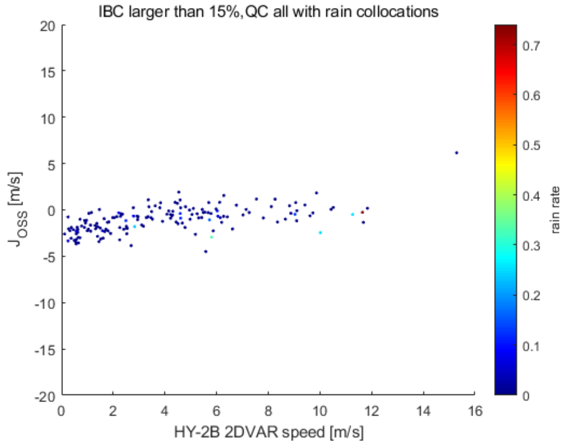

Sorted by Joss: (a) IBC (b) SIC (c) MLE (d) Rain rate

IBC >=15%

Ku band scatterometer MLE and Joss v.s. SAR iceberg

- *Statistics (averaged view)*

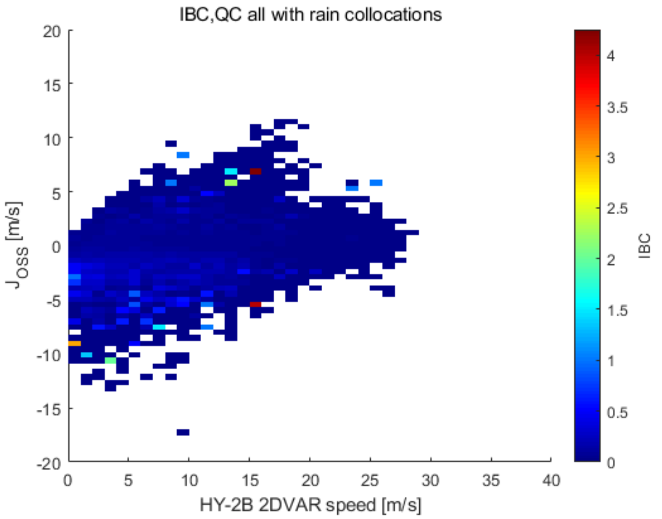

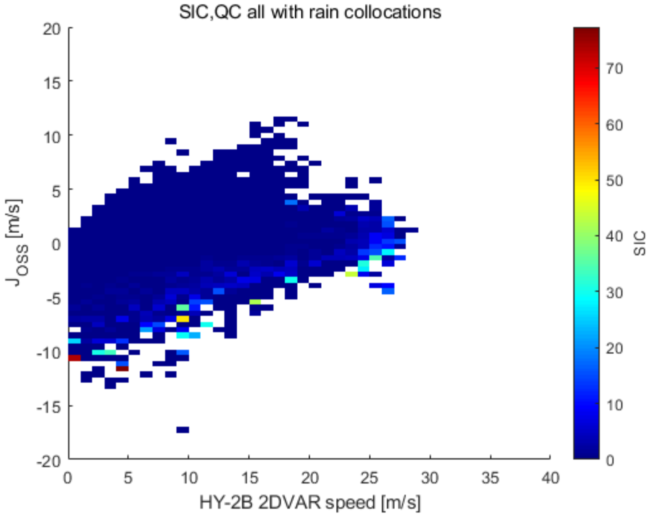

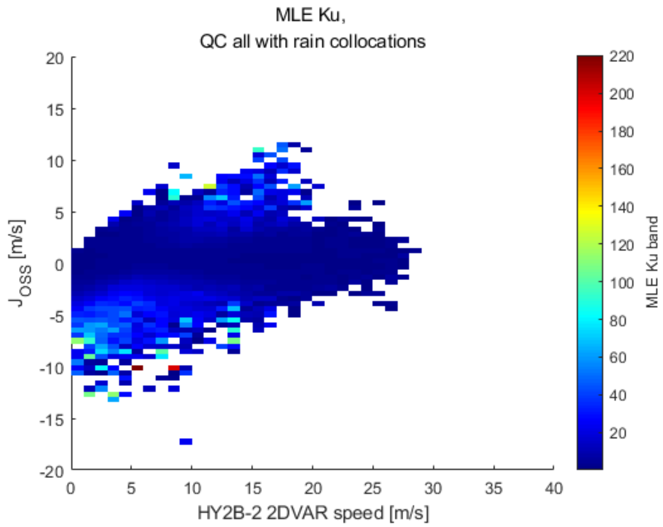

Sorted by Joss: (a) IBC (b) SIC (c) MLE

(d) Rain rate

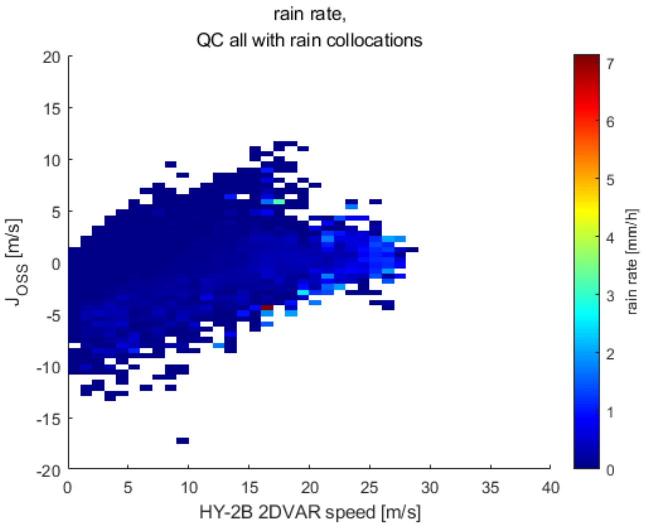

(e) Density

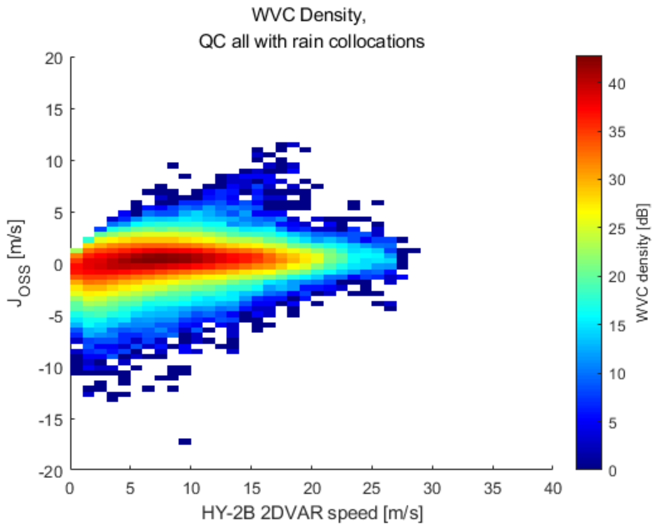

IBC >=15% curve corresponding to large density

Conclusions and Discussions

- Conclusions:
  - Bayesian scatterometer sea ice screening is operational
  - In the collocation set, the ice screening ability of J_{oss} in addition to *MLE* has been confirmed
  - Combined C and Ku band is favorable in discriminating rain and sea ice effects
  - Iceberg is in smaller scales different from SIC. Though iceberg induce larger signal return, they require better spatial resolution in measurement, and better resolved by MLE.
  - Inclusion of precipitation probability could improve ice Bayesian.

- Further Research:
  - NRCS features due to mixed ice, icebergs and open ocean

(X. Xu and A. Stoffelen, 2003)

Key References

- M. Belmonte Rivas, J. Verspeek, A. Verhoef and A. Stoffelen, "Bayesian Sea Ice Detection With the Advanced Scatterometer ASCAT," in IEEE Transactions on Geoscience and Remote Sensing, vol. 50, no. 7, pp. 2649-2657, July 2012, doi: 10.1109/TGRS.2011.2182356.
- M. Belmonte Rivas and A. Stoffelen, "New Bayesian Algorithm for Sea Ice Detection With QuikSCAT," in IEEE Transactions on Geoscience and Remote Sensing, vol. 49, no. 6, pp. 1894-1901, June 2011, doi: 10.1109/TGRS.2010.2101608.
- A. Stoffelen and M. Portabella, "On Bayesian scatterometer wind inversion," in IEEE Transactions on Geoscience and Remote Sensing, vol. 44, no. 6, pp. 1523-1533, June 2006, doi: 10.1109/TGRS.2005.862502.

- M. Belmonte Rivas and A. Stoffelen, "New Bayesian Algorithm for Sea Ice Detection With QuikSCAT," in IEEE Transactions on Geoscience and Remote Sensing, vol. 49, no. 6, pp. 1894-1901, June 2011, doi: 10.1109/TGRS.2010.2101608.

- J. Verspeek, A. Stoffelen, M. Portabella, H. Bonekamp, C. Anderson and J. F. Saldana, "Validation and Calibration of ASCAT Using CMOD5.n," in IEEE Transactions on Geoscience and Remote Sensing, vol. 48, no. 1, pp. 386-395, Jan. 2010, doi: 10.1109/TGRS.2009.2027896.
- J. Vogelzang, A. Stoffelen, A. Verhoef and J. Figa-Saldaña, On the quality of high-resolution scatterometer winds, J. Geophys. Res., 116, C10033, 2011. doi:10.1029/2010JC006640.
- X. Xu and A. Stoffelen, "Improved Rain Screening for Ku-Band Wind Scatterometry," IEEE Transactions on Geoscience and Remote Sensing, vol. 58, no. 4, pp. 2494-2503, 2020, doi: 10.1109/tgrs.2019.2951726.
- X. Xu, A. Stoffelen, and J. F. Meirink, "Comparison of Ocean Surface Rain Rates From the Global Precipitation Mission and the Meteosat Second-Generation Satellite for Wind Scatterometer Quality Control," IEEE Journal of Selected Topics in Applied Earth Observations and Remote Sensing, vol. 13, pp. 2173-2182, 2020, doi: 10.1109/jstars.2020.2995178.
- X. Xu and A. Stoffelen, "Sea Ice Screening Ability in Ku-Band and C-Band Wind Scatterometry," IGARSS 2023 - 2023 IEEE International Geoscience and Remote Sensing Symposium, Pasadena, CA, USA, 2023, pp. 4088-4091, doi: 10.1109/IGARSS52108.2023.10283179.

中国科学院国家空间科学中心
National Space Science Center . CAS

Koninklijk Nederlands
Meteorologisch Instituut
Ministerie van Infrastructuur en Waterstaat

Thanks!